Bubble Convection Experiments with a Semi-implicit Formulation of the Euler Equations

ANDRÉ ROBERT

Département de Physique, Université du Québec, Montreal, Quebec, Canada

(Manuscript received 7 October 1991, in final form 27 July 1992)

ABSTRACT

Atmospheric models based on the Euler equations exist and are used occasionally to carry out numerical experiments. Such a model is used here to simulate the motion of warm bubbles in a dry isentropic atmosphere. For the time integration, this model uses a scheme that is semi-Lagrangian and semi-implicit. It is the stability and the efficiency of this integration scheme that is examined in the context of an isentropic vertical stratification. Some results are presented and are compared with the results generated by similar experiments reported in the scientific literature.

1. Introduction

Atmospheric models rarely use the full meteorological equations. The reason for this is that these equations contain high-frequency sound waves. These waves impose a severe restriction on the size of the time step that can be used in order to produce stable integrations. The most common practice consists in using approximations that eliminate sound waves from the equations. Large-scale models use the hydrostatic approximation. Convection models generally use the anelastic approximation.

There are a few models that use the complete meteorological equations. These are called compressible fluid models, and they use the Euler equations. The main characteristic of these models is that they include sound waves. Both the hydrostatic approximation and the anelastic approximation are avoided. The problem with these models is that they can be very time consuming, even on present supercomputers. In order to partially avoid this problem, these models use specialized integration schemes designed to produce stable integrations with fewer calculations than the amount required with classical integration algorithms.

One technique consists of using the split-explicit scheme proposed by Gadd (1978). This technique separates the terms in the equations in such a way that sound waves are integrated with a short time step while other waves are integrated with a larger time step. The split-explicit method is also used by Klemp and Wilhelmson (1978) and by Cotton and Tripoli (1978) in models of the Euler equations that are used to perform experiments at convective scales.

Another method consists of using the semi-implicit scheme proposed by Robert (1969). Such a scheme is used by Tapp and White (1976) and also by Tanguay et al. (1990) in models of the Euler equations. This latter article will be called TRL in subsequent references.

In the model of Tapp and White, the semi-implicit formulation is applied to sound waves, and the model is used to produce short-range mesoscale weather forecasts. In TRL, the Euler equations are used on a nearly hemispheric scale, and the semi-implicit scheme is applied to both sound waves and gravity waves.

In principle, it seems that this model could be used at any other meteorological scale. In order to test this hypothesis, the model is applied to bubble convection in an isentropic environment. It is unclear whether the semi-implicit scheme will function properly under these conditions. In order to remain stable, this technique must satisfy a number of constraints. The most important constraint is related to the reference state used in the model for the application of the semi-implicit scheme. This question has been investigated by Simmons et al. (1978). In their investigations, they found that the semi-implicit scheme develops numerical instability in the polar regions if the static stability of the model reference state is too low. In their paper, they recommend an isothermal reference state.

In another study, Côté et al. (1983) arrive at the same conclusion, but their analysis implies that it is the computational mode associated with the leapfrog scheme that is the most unstable. Both papers maintain that a positive definite model static stability is insufficient to guarantee stability. Both papers give the same necessary condition for stability.

Corresponding author address: Dr. André Robert, Department de Physique, Université du Québec, Case Postale 8888, Succ. A., Montreal, Quebec, Canada, H3C 3P8.

Similarly, it seems also that the semi-implicit scheme might run into difficulties if the static stability vanishes at some point in the atmosphere or if it becomes negative. Large-scale models use a parameterized convective adjustment scheme that constrains the static stability to positive values. This constraint is applied in all large-scale models including those that use classical integration algorithms. It is used to prevent a form of instability that would otherwise be well managed if the resolution of the model could be extended all the way to a scale of a few meters. If we wish to test the performance of the semi-implicit scheme in an isentropic atmosphere, we should displace ourselves to the convective scale where the adjustment constraint on static stability is not needed. This is done in the following sections.

2. Description of the model

The Euler equations are used in the following vectorial form:

$$\frac{d\mathbf{C}}{dt} = \mathbf{B}, \tag{1}$$

where the vector $\mathbf{C}$ has the following components,

$$\mathbf{C} = (u, v, w, q', T'), \tag{2}$$

and the five components of the vector appearing on the right-hand side of (1) are given as

$$B_1 = -RT\frac{\partial q'}{\partial x} \tag{3}$$

$$B_2 = -RT\frac{\partial q'}{\partial y} \tag{4}$$

$$B_3 = -RT\frac{\partial q'}{\partial z} + \frac{gT'}{T^*} \tag{5}$$

$$B_4 = -\frac{D}{1-\kappa} + \frac{gw}{RT^*} \tag{6}$$

$$B_5 = -\frac{\kappa T}{1-\kappa} D \tag{7}$$

$$D = \frac{\partial u}{\partial x} + \frac{\partial v}{\partial y} + \frac{\partial w}{\partial z} \tag{8}$$

$$q' = q - q^* \tag{9}$$

$$T' = T - T^*. \tag{10}$$

In these equations T^* is a constant, and

$$q^* = -\frac{gz}{RT^*} \tag{11}$$

$$q = \ln\left[\frac{p}{p_0}\right] \tag{12}$$

$$p_0 = 1000 \text{ mb} \tag{13}$$

$$\kappa = \frac{R}{C_p} = \frac{2}{7}. \tag{14}$$

The gas constant R is for dry air; u, v, and w are the three components of the wind; p is pressure; and T is the temperature. A complete derivation of this form of the Euler equations is given in TRL. Adiabatic motion is considered, and the terms arising from the rotation and sphericity of the earth are omitted.

These equations are nearly in the form used by the semi-implicit scheme. In order to complete the transformation, we define another vector $\mathbf{B}^*$ as follows:

$$B_1^* = -RT^*\frac{\partial q'}{\partial x} \tag{15}$$

$$B_2^* = -RT^*\frac{\partial q'}{\partial y} \tag{16}$$

$$B_3^* = -RT^*\frac{\partial q'}{\partial z} \tag{17}$$

$$B_4^* = -\frac{D}{1-\kappa} \tag{18}$$

$$B_5^* = -\frac{\kappa T^*}{1-\kappa} D, \tag{19}$$

and finally,

$$\mathbf{B}' = \mathbf{B} - \mathbf{B}^*, \tag{20}$$

so that our original differential equation may now be written as follows:

$$\frac{d\mathbf{C}}{dt} = \mathbf{B}^* + \mathbf{B}'. \tag{21}$$

Up to this point, all manipulations were made without any approximations. The first approximation will consist in applying the discretization that generates the semi-Lagrangian and semi-implicit technique:

$$\frac{d\mathbf{C}}{dt} = \overline{\mathbf{B}^*}^t + \mathbf{B}'. \tag{22}$$

Here, the various symbols are defined as follows:

$$\frac{dF}{dt} = \frac{F[r^+, t+\Delta t] - F[r^-, t-\Delta t]}{2\Delta t} \tag{23}$$

$$\bar{F}^t = \frac{F[r^+, t+\Delta t] + F[r^-, t-\Delta t]}{2} \tag{24}$$

$$F = F(r^0, t), \tag{25}$$

where

$$r^+ = (x, y, z) \tag{26}$$

$$r^0 = (x-\alpha, y-\beta, z-\gamma) \tag{27}$$

$$r^- = (x-2\alpha, y-2\beta, z-2\gamma) \tag{28}$$

and

$$\alpha = \Delta t u(r^0, t) \tag{29}$$

$$\beta = \Delta t v(r^0, t) \tag{30}$$

$$\gamma = \Delta t w(r^0, t). \tag{31}$$

In the preceding equations, r^+ is a grid point, while r^0 and r^- are upstream points along a trajectory defined by the wind at the midpoint of the three-point trajectory. All quantities that need to be determined at upstream points are computed with a multiply upstream tricubic interpolator in three dimensions. This algorithm naturally reduces to bicubic interpolation in two dimensions. The multiply upstream characteristic is quite important for stability when the points are far upstream. The interpolation is always carried out from the grid points that are nearest to the upstream point.

The stability constraint in the TRL model due to an Eulerian treatment of vertical advection is removed by adopting semi-Lagrangian advection in all space dimensions.

The manipulations required for the integration of (22) are described in TRL as well as in many other papers that describe the semi-implicit method. These descriptions will not be repeated here.

The spatial discretization uses the Arakawa-C type of staggering. For instance, along the x axis, a first set of grid points is defined in the interval

$$0 \leq x \leq L \tag{32}$$

as follows:

$$x_i = (i - 1)\Delta x, \tag{33}$$

where i is an integer such that

$$1 \leq i \leq NI \tag{34}$$

and

$$\Delta x = \frac{L}{NI - 1}. \tag{35}$$

The wind component u along the x axis is defined at these grid points. All other variables are defined on the following set of points:

$$x_i = \left(i - \frac{1}{2}\right)\Delta x \tag{36}$$

with

$$1 \leq i \leq NI - 1, \tag{37}$$

and Δx is as previously defined.

The same principle is applied also in the other two dimensions so that we end up with a total of eight regular grids, all staggered with respect to each other. Only four of these grids are effectively used to represent the dependent variables. The main advantage of this discretization is that all derivatives are evaluated over a distance of one grid length. The disadvantage is that some variables must be averaged over a distance of one grid length. At present, two-point second-order approximations are used everywhere. In practice, it is the semi-implicit scheme that benefits most from this type of staggering.

For the semi-Lagrangian part of the model, the staggered velocity components are averaged to the grid centers, and the displacements applicable to these points are computed. These displacements are used to compute the upstream values of the terms related to pressure and temperature (components 4 and 5 of the corresponding vectors). For the other three variables (u, v, and w), the displacements computed above are averaged to the three corresponding grids for the computation of upstream values. In other words, upstream values of a quantity expressed on a given grid are always computed with the help of displacements averaged to this grid.

3. The bubble convection experiments

The experiments reported in this section are carried out in two dimensions, even though the model can run in three dimensions. A mesh length of 10 m and a time step of 5 sec will be used. The basic-state atmosphere will be isentropic with a potential temperature of 30°C. Initially it will be at rest and in hydrostatic equilibrium. The semi-implicit scheme uses a reference temperature T^* of 30°C.

In the first experiment, a domain of 1 km by 1 km is used and is enclosed within solid walls. A circular bubble with a diameter of 500 meters will be considered. The bottom of the bubble will be positioned 10 meters above the underlying surface. The bubble will be assigned a uniform potential temperature of 30.5°C, which is 0.5°C in excess of the environmental potential temperature. The environmental pressure will not be altered so that initially all the air parcels within the bubble will be subjected to a small buoyancy force.

The results of the corresponding integration are presented at $t = 7$ min in Fig. 1 and at $t = 10$ min in Fig. 2. These charts show the distribution of potential temperature. These results will be compared with those of a similar experiment carried out by Smolarkiewicz and Grabowski (1990) using the anelastic model of Clark (1977). Their Fig. 7 plots the potential temperature at $t = 10$ min. It should be noted that their domain is only 800 m wide. Other differences are in the models that were used. There is some large-scale resemblance between the patterns, but there are significant differences in the smaller scales. The results of Smolarkiewicz and Grabowski are noisy. This is not the case with the proposed model in spite of the fact that it did not use any explicit time filter or diffusion.

Another similar experiment was performed by Smolarkiewicz and Pudykiewicz (1992). In this case, the Boussinesq equations were used with a semi-La-

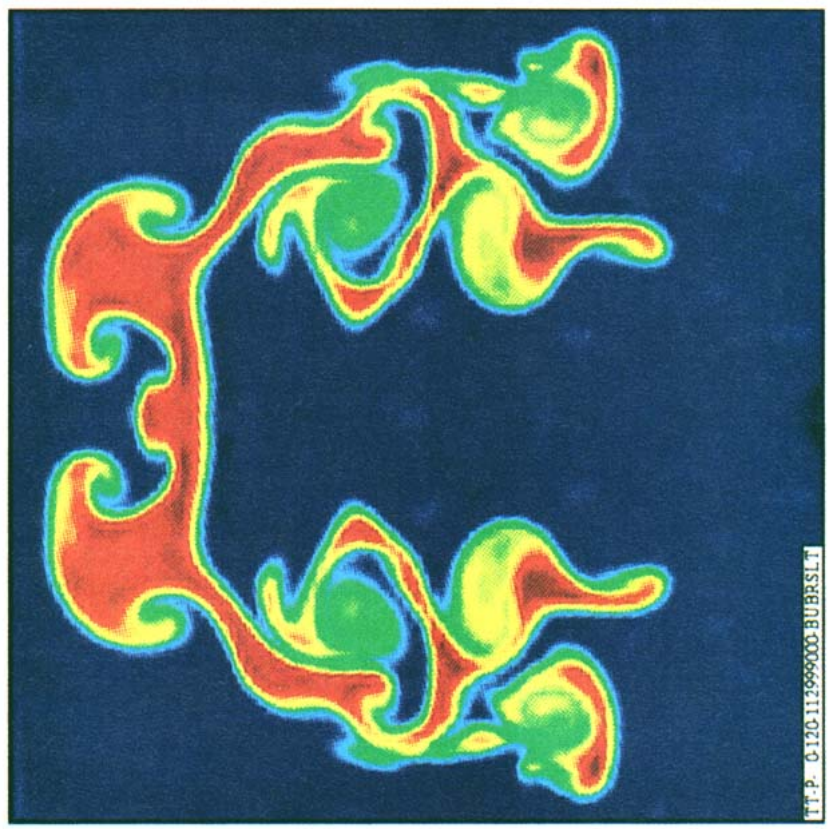

FIG. 2. Same as Fig. 1 but at $t = 10$ min.

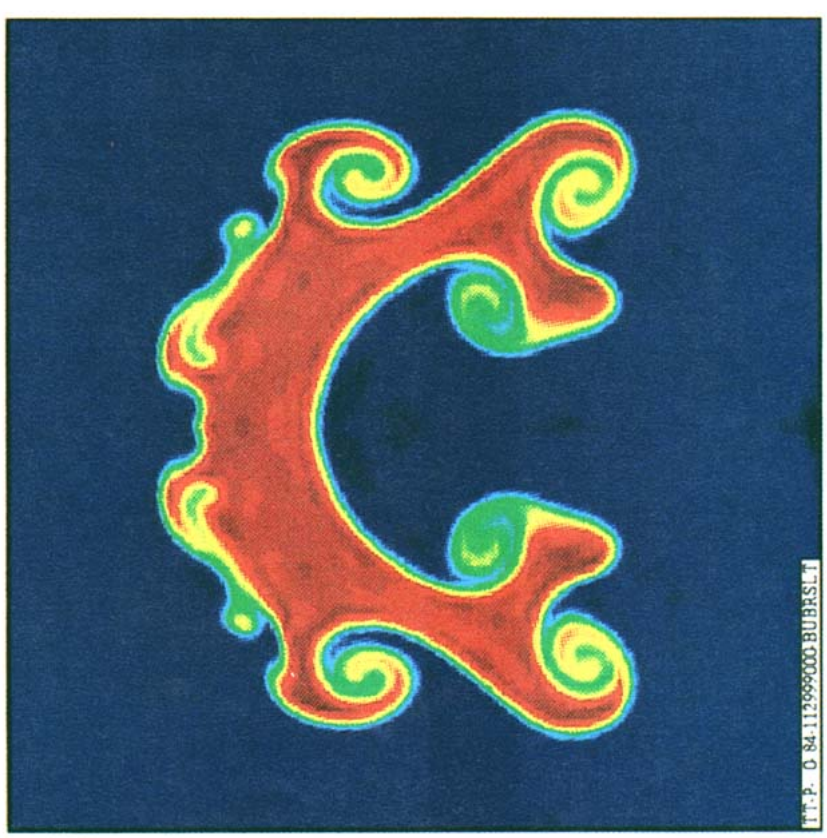

FIG. 1. Potential temperature distribution at $t = 7$ min for an initially circular bubble with a diameter of 500 m and uniform potential temperature excess of 0.5°C over an isentropic environment.

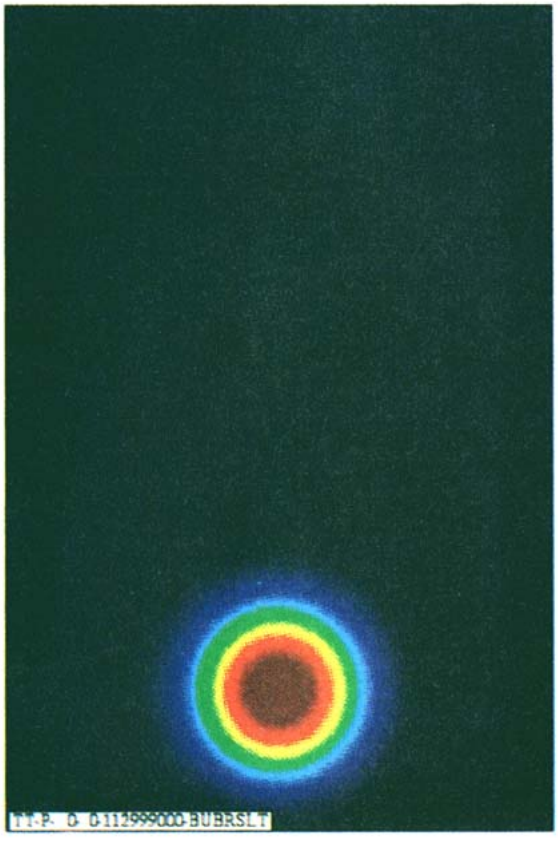

FIG. 3. Potential temperature distribution at $t = 0$ for a circular bubble with a Gaussian profile in an isentropic environment.

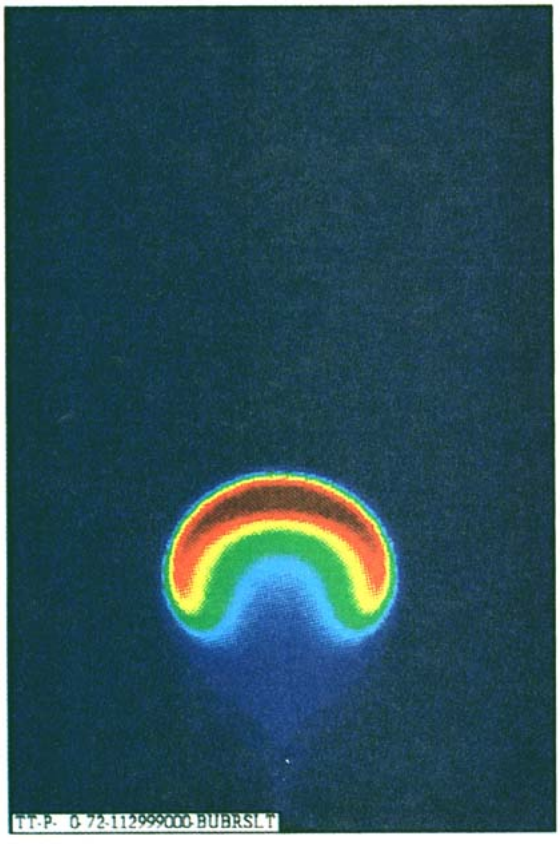

FIG. 4. Same as Fig. 3 but at $t = 6$ min.

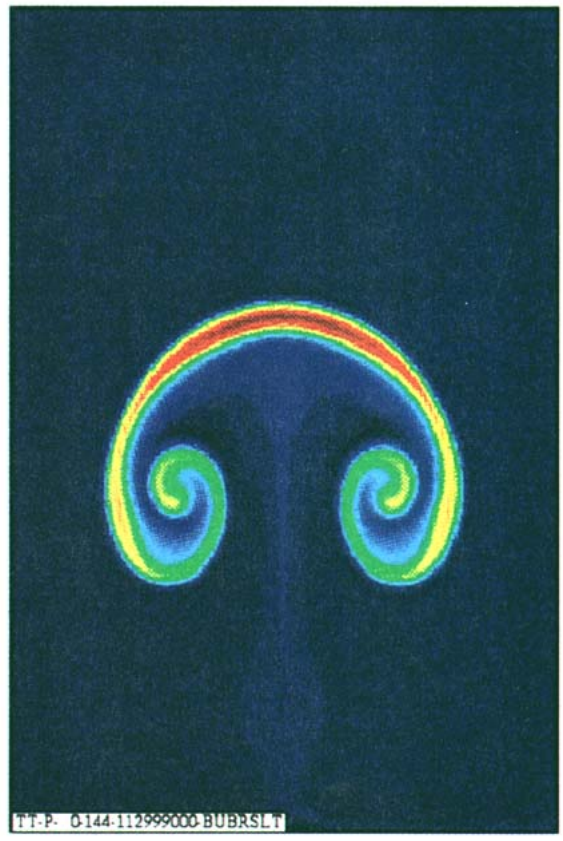

FIG. 5. Same as Fig. 3 but at $t = 12$ min.

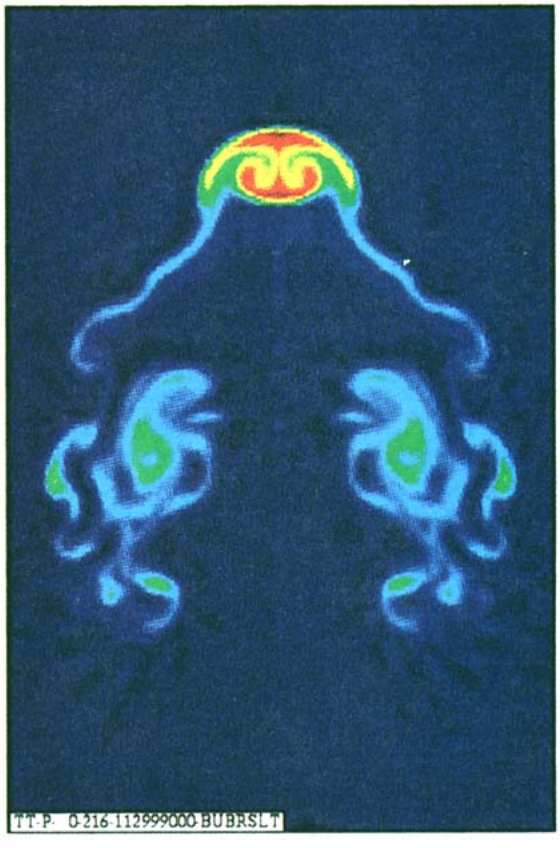

FIG. 6. Same as Fig. 3 but at $t = 18$ min.

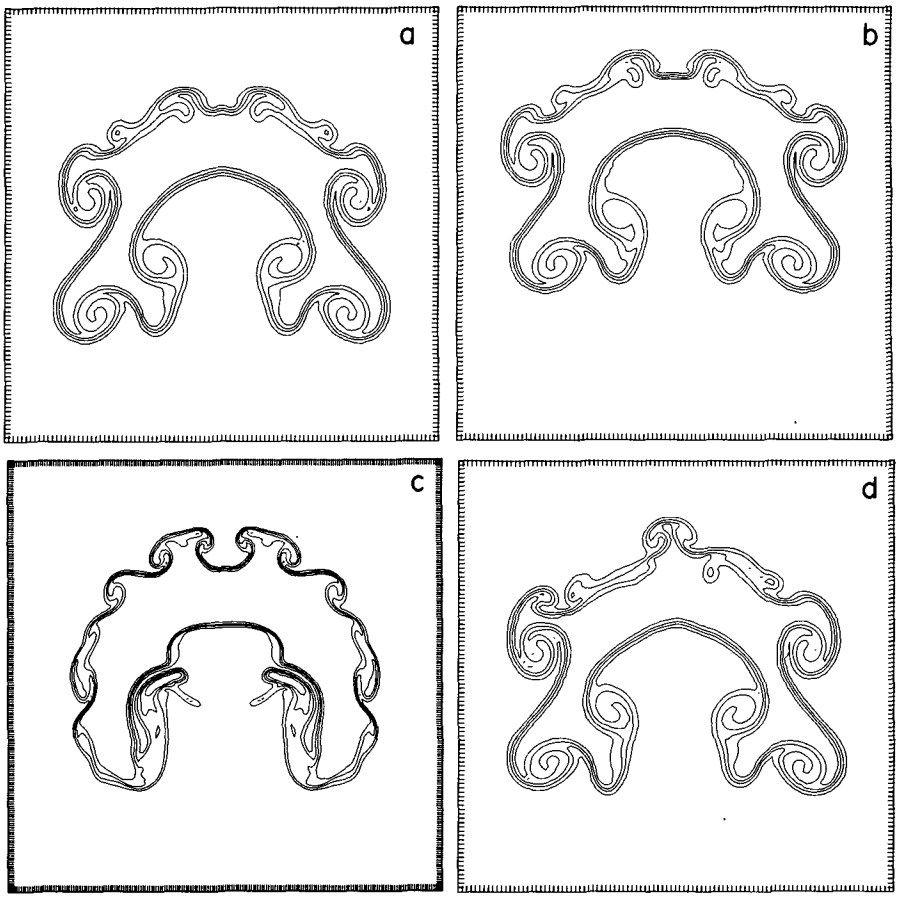

FIG. 7. As in Fig. 1. (a) Regular run with a mesh length of 10 m and a time step of 5 sec over a 1-km by 1-km domain; (b) same window over a domain enlarged to 2 km by 2 km, (c) mesh length and time step reduced to 5 m and 2.5 sec over the 1-km by 1-km domain; (d) regular run with weak random noise added to the initial potential temperature.

grangian discretization. They also enlarged their domain to 2 km × 2 km.

They plot the potential temperature after 7.2 min in their Fig. 3b and after 10 min in Fig. 3c. In this case there is a much greater resemblance, especially at $t = 7$ min. Comparable vortices show up clearly, as in Fig. 1 of this paper. A fraction of the bubble of Smolarkiewicz and Pudykiewicz shows up above the 750-m level. A slightly smaller fraction of the bubble of Fig. 1 also shows up above the 750-m level. The presence of a lid at a height of 1 km seems to have a small impact on the results at 7 min.

Another experiment is carried out with a different type of bubble. In this case, the distribution of potential temperature within the bubble is given by

$$\theta = \begin{cases} A, & r \leq a \\ Ae^{-(r-a)^2/s^2}, & r > a, \end{cases} \tag{38}$$

with

$$r^2 = (x - x_0)^2 + (z - z_0)^2. \tag{39}$$

This produces a bubble with a Gaussian profile. A small flat region is added at the center; $A = 0.5°C$, $a = 50$ m, $s = 100$ m, $x_0 = 500$ m, and $z_0 = 260$ m. The results of the corresponding integration are presented in Figs. 3, 4, 5, and 6. The plots correspond to $t = 0$, 6, 12, and 18 min. It should be noted that the upper boundary has been moved to a height of 1500 m.

A similar experiment was carried out by Carpenter et al. (1988) using a model of the Euler equations with very short time steps. They present potential temperature at $t = 10$ min in their Fig. 9b and at 14 min in Fig. 9c. Their patterns are comparable to those of Fig. 5 except that they are slightly more noisy. Carpenter et al. also examined the influence of spatial resolution on their results. They find that fairly intense Kelvin–Helmholtz waves appear along the sharp edge of the bubble when the resolution is increased. In this latter study, they indicate that a time step of 0.4 sec with a mesh length of 20 m was used. A comparable run with the proposed semi-implicit formulation would require a time step six times longer.

Another similar integration is reported by Nickerson

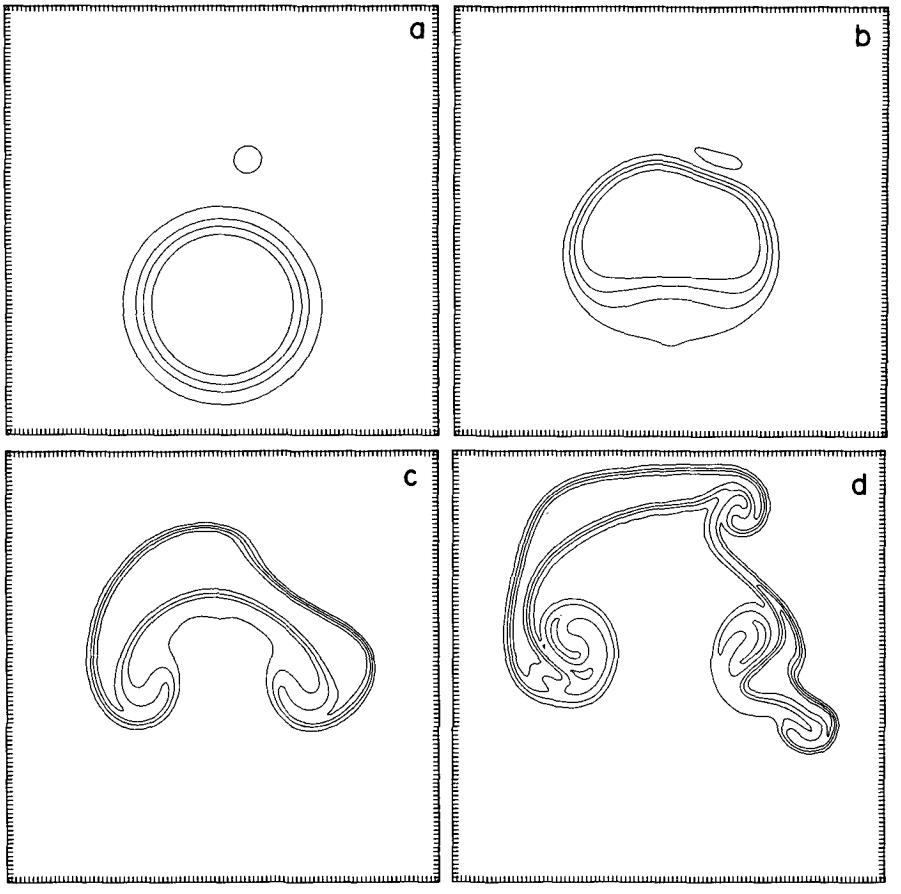

FIG. 8. Potential temperature distribution at t = 0, 4, 7, and 10 min for a run with a large warm bubble and a small cold bubble as initial conditions as depicted in panel (a) for mesh length 10 m and time step 5 sec.

(1965). He presents results at t = 2, 6, and 10 min in his Figs. 3, 4, and 5. His results are very smooth. He uses only a half bubble since the lower half has been deleted. This makes comparisons more difficult, but on the other hand, the overall behavior of his bubble does not differ significantly from the results of Carpenter et al. or those reported in this paper.

At this point, some of the results presented earlier will be reexamined. The charts presented by Smolarkiewicz and Grabowski (1990) are noisy, but smooth results are presented by Smolarkiewicz and Pudykiewicz (1992) when a monotonicity constraint is used. Without this constraint, they obtain noisy results, as shown in their Fig. 4a. Since the semi-Lagrangian scheme used in this paper does not apply any monotonicity constraint, it could be argued that it must necessarily produce noise that is hidden by a color presentation that would show only slight differences in shades of the same color in the presence of noise.

In order to test this hypothesis, a contour display of Fig. 1 is presented in Fig. 7a. This display will be used also to compare the results of a few sensitivity experiments that will be presented here. It can easily be seen that the results of Fig. 7a are smooth, indicating that the proposed semi-Lagrangian scheme does not need a monotonicity constraint for smoothness. The main reason for this is that the proposed semi-Lagrangian scheme contains some inherent diffusion arising from the bicubic interpolation procedure. On the other hand, it must be recognized that a monotonicity constraint can effectively remove overshoots and undershoots that will inevitably occur in any unconstrained cubic interpolation scheme. The largest unphysical anomaly observed in the potential temperature of Fig. 7a is an undershoot of 0.016°C that occurs slightly below the bottom of the bubble.

The bubble of Fig. 1 is slightly lower than that of Smolarkiewicz and Pudykiewicz, and this is probably due to the presence of a lid at a height of 1 km. This can easily be verified by enlarging the domain to 2 km by 2 km without changing the resolution of the model. The corresponding result is presented over the original window in Fig. 7b, and it can easily be seen that the top of the bubble is about 80 m higher. Over this enlarged domain, the position of the bubble is closer to that of Smolarkiewicz and Pudykiewicz.

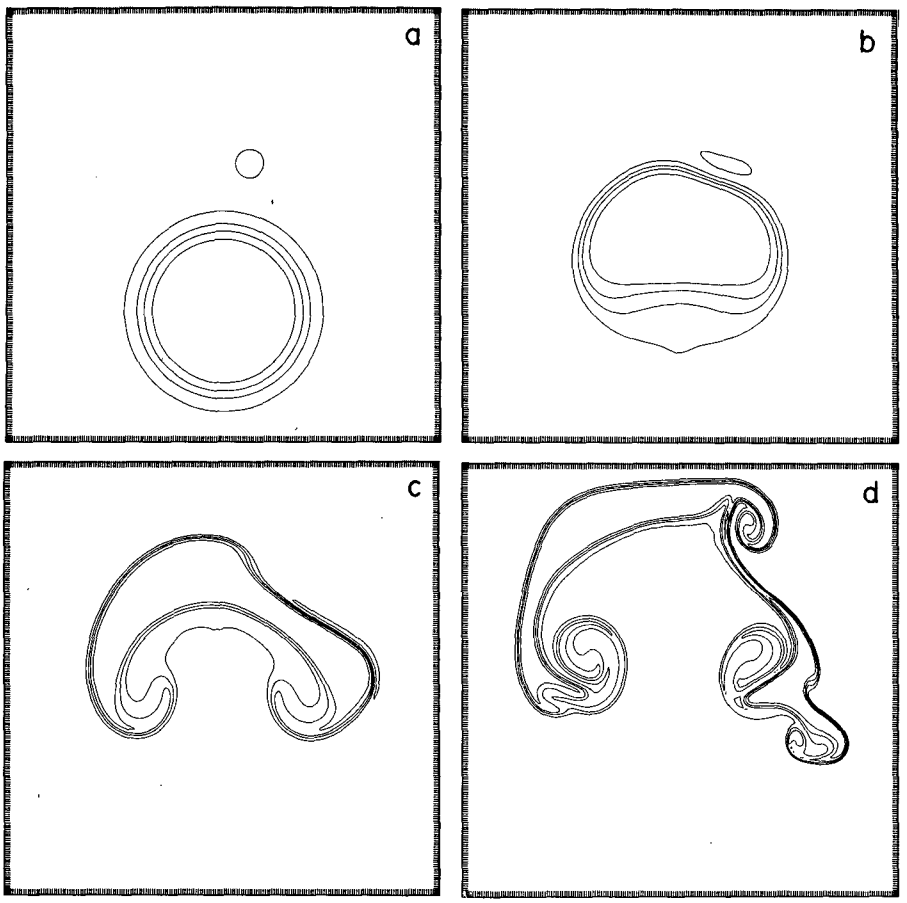

FIG. 9. Same as Fig. 8 but with the mesh length and time step reduced to 5 m and 2.5 sec.

The main question that always arises when the results of numerical experiments are presented is the question of accuracy. In the absence of a known analytic solution, as is the case here, it is not easy to address this question. The easiest thing that can be done is to determine if the integration is sensitive to the resolution used. For this purpose the resolution is doubled in both space and time. The corresponding result is shown in Fig. 7c. It is obvious here that the behavior is quite different, indicating that the resolution used in the model is inadequate.

Finally, the sensitivity of the model to the initial conditions is tested. For this purpose, background noise is added, randomly distributed in the interval ± 0.025°C. This noise is added to the initial potential temperature. The resulting integration, presented in Fig. 7d, does not show any significant differences over the bottom two-thirds of the bubble. It is essentially near the top that the configurations are significantly different, indicating that this is the most unstable region of the bubble.

It has not yet been demonstrated that the model is able to produce accurate results. A uniform bubble with a sharp edge cannot be used for this purpose because the local truncation errors near the edge are large and remain large whatever resolution is used. Furthermore, the scale of the vortices generated along the edge becomes smaller when the resolution is increased, and it seems that this process will continue until a very small scale is reached where molecular diffusion becomes important.

In order to estimate the accuracy of the model, it is preferable to consider an initial state where the fields have a well-defined scale that can be resolved by an appropriate grid. In other words, it is preferable to consider bubbles with a Gaussian profile or any other reasonably smooth profile. An initial state that contains two bubbles is considered. The first one is warm with $A_1 = 0.5$°C, $a_1 = 150$ m, $S_1 = 50$ m, $x_1 = 500$ m, and $z_1 = 300$ m. The second bubble is cold with $A_2 = -0.15$°C, $a_2 = 0$, $S_2 = 50$ m, $x_2 = 560$ m, and $z_2 = 640$ m. This pattern contains one reasonably large scale element, as can be seen in Fig. 8a at the initial time. It contains also some elements with a smaller characteristic scale of the order of 50 m or $5\Delta x$. Models can handle smaller scales than this, but we must allow for the fact that this smaller characteristic scale will be reduced progressively as the integration proceeds. This

is evidenced in Figs. 8b,c,d, showing the results of the integration after 4, 7, and 10 min. In some places, the edge of the large bubble becomes sharper with time. The vortices that show up at $t = 10$ min (Fig. 8d) may still depend on the resolution used by the model. In order to check this point, the resolution is doubled in both space and time and the model is run again from the same initial conditions. The corresponding result is presented in Fig. 9. It is evident from Fig. 8b and Fig. 9b that dependence on the model resolution is negligible at $t = 4$ min. It is also clear from Figs. 8c and 9c that the differences are still relatively small at $t = 7$ min. It is only at $t = 10$ min that the differences become more evident. The edges of the patterns are sharper, and the vortices contain more pronounced details in the higher-resolution run. On the other hand, if Figs. 8d and 9d were superposed, we would find that the positions of the vortices coincide as well as the general outlines of the other patterns. In other words, the large-scale patterns are nearly identical, while small-scale features are only slightly different. This is in sharp contrast with the results presented earlier in Figs. 7a,c at $t = 7$ min.

4. Conclusions

It seems that a semi-implicit formulation of the Euler equations works quite well at the convective scale in an atmosphere where the static stability vanishes. There are no obvious signs of numerical instability in the integrations. The results are comparable with those of an anelastic model, a model of the Boussinesq equations, and a model of the Euler equations with a classical integration scheme. The closest resemblance occurs when Fig. 1 of this paper is compared with Fig. 3b of Smolarkiewicz and Pudykiewicz (1992).

With a semi-implicit scheme, the Euler equations can be integrated with a much larger time step. The resulting model even runs with a time step larger than normally used in anelastic or Boussinesq models. It is also as efficient as these models since most of the computer time is used by the semi-Lagrangian advection and the solution of an elliptic equation that is common to all models. The only advantage of a model based on the Euler equations is that it is universal in the sense that it can be used at all meteorological scales. This is an important property since it means that it is no longer necessary to design two different models for two different applications. It becomes possible to use a single model for all applications, and this can be done without any loss of efficiency.[1]

REFERENCES

Carpenter, R. L., Jr., K. K. Droegemeier, P. R. Woodward, and C. E. Hane, 1988: Application of the piecewise parabolic method (PPM) to meteorological modeling. Proc. *Eighth Conf. on Numerical Weather Prediction,* Baltimore, Amer. Meteor. Soc. 791–798.

——, ——, ——, and ——, 1990: Application of the piecewise parabolic method (PPM) to meteorological modeling. *Mon. Wea. Rev.,* **118,** 586–612.

Clark, T. L., 1977: A small scale numerical model using a terrain following coordinate system. *J. Comput. Phys.,* **24,** 186–215.

Côté, Jean, Michel Béland and Andrew Staniforth, 1983: Stability of vertical discretization schemes for semi-implicit primitive equation models: Theory and application. *Mon. Wea. Rev.,* **111,** 1189–1207.

Cotton, W. R., and G. J. Tripoli, 1978: Cumulus convection in shear flow three-dimensional experiments. *J. Atmos. Sci.,* **35,** 1503–1521.

Gadd, A. J., 1978: A split-explicit integration scheme for numerical weather prediction, *Quart. J. Roy. Meteor. Soc.* **104,** 569–582.

Klemp, J. B., and R. Wilhelmson, 1978: The simulation of three-dimensional convective storm dynamics. *J. Atmos. Sci.,* **35,** 1070–1096.

Nickerson, E. C., 1965: A numerical experiment in buoyant convection involving the use of a heat source. *J. Atmos. Sci.,* **22,** 412–418.

Robert, A. J., 1969: The integration of a spectral model of the atmosphere by the implicit method. Proc. *WMO-IUGG Symp. on NWP,* Tokyo, Japan Meteorological Agency, VII, 19–24.

Simmons, A. J., B. J. Hoskins, and D. M. Burridge, 1978: Stability of the semi-implicit method of time integration. *Mon. Wea. Rev.,* **106,** 405–412.

Smolarkiewicz, P. K., and W. W. Grabowski, 1990: The multidimensional positive definite advection transport algorithm: Nonoscillatory option. *J. Comput. Phys.,* **86,** 355–375.

——, and J. A. Pudykiewicz, 1992: A class of semi-Lagrangian approximations for fluids. *J. Atmos. Sci.,* **49,** 2082–2096.

Tanguay, M., A. Robert, and R. Laprise, 1990: A semi-implicit semi-Lagrangian fully compressible regional forecast model. *Mon. Wea. Rev.,* **118,** 1970–1980.

Tapp, M., and P. W. White, 1976: A non-hydrostatic mesoscale model. *Quart. J. Roy. Meteor. Soc.,* **102,** 277–296.

[1] The Fortran code for this model is available on a Macintosh diskette, and copies will be provided free of charge upon request.